JACS
JOURNAL OF THE AMERICAN CHEMICAL SOCIETY
Article
pubs.acs.org/JACS

New Insights on Photocatalytic H_2 Liberation from Water Using Transition-Metal Oxides: Lessons from Cluster Models of Molybdenum and Tungsten Oxides

Raghunath O. Ramabhadran, Jennifer E. Mann, Sarah E. Waller, David W. Rothgeb, Caroline C. Jarrold, and Krishnan Raghavachari*

Department of Chemistry, Indiana University, Bloomington, Indiana 47405, United States

Supporting Information

ABSTRACT: Molecular hydrogen (H_2) is an excellent alternative fuel. It can be produced from the abundantly present water on earth. Transition-metal oxides are widely used in the environmentally benign photocatalytic generation of H_2 from water, thus actively driving scientific research on the mechanisms for this process. In this study, we investigate the chemical reactions of $W_3O_5^-$ and $Mo_3O_5^-$ clusters with water that shed light on a variety of key factors central to H_2 generation. Our computational results explain why experimentally $Mo_3O_5^-$ forms a unique kinetic trap in its reaction while $W_3O_5^-$ undergoes a facile oxidation to form the lowest-energy isomer of $W_3O_6^-$ and liberates H_2. Mechanistic insights on the reaction pathways that occur, as well as the reaction pathways that do not occur, are found to be of immense assistance to comprehend the hitherto poorly understood pivotal roles of (a) differing metal−oxygen and metal−hydrogen bond strengths, (b) the initial electrostatic complex formed, (c) the loss of entropy when these TMO clusters react with water, and (d) the geometric factors involved in the liberation of H_2.

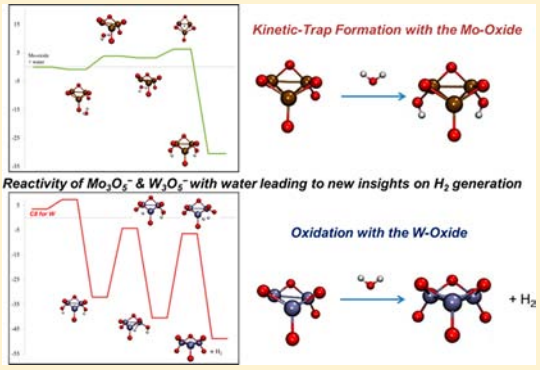

INTRODUCTION

Growing world population and active concerns of climate change have propelled a huge scientific interest toward alternate energy sources.[1] Molecular hydrogen, possessing several lucrative features such as an outstanding energy density by mass (143 MJ/kg), excellent eco-friendliness, and the ready availability of a feedstock (H_2O), is clearly an important alternative fuel.[2,3]

Out of the various possible methods of manufacturing H_2 from water, photocatalytic generation of H_2 from water has received widespread attention in recent years as it does not rely on fossil fuels and leads to no carbon dioxide emission.[4−9] Furthermore, transition-metal oxides (TMOs) have been found to be particularly efficient in carrying out the photocatalytic splitting of water.[10−18]

The surface defects on TMO systems that are principally responsible for their photocatalytic actions can be adequately represented by cluster models.[19] It is well-established that experimental and computational gas-phase studies on neutral and ionic TMO clusters are very useful to identify the active sites in chemical reactions pertinent to alternate energy production.[20−22]

A variety of studies on TMO clusters[23−81] have been performed by many groups with the goal of advancing their applications in heterogeneous catalysis.[82−87] In a combined computational and mass spectrometry/photoelectron spectroscopy study, we had recently studied H_2 production from small $W_2O_y^-$ (y = 2−6) clusters.[88] Besides, it was also experimentally observed that in reactions between $W_3O_5^-$ and $Mo_3O_5^-$ clusters with H_2O, molybdenum oxide forms a $Mo_3O_6H_2^-$ kinetic trap, whereas the tungsten oxide shows a propensity to generate H_2.[89] These exploratory studies were useful in identifying the reactive sites in small clusters leading to a pathway conducive to H_2 production as well as experimental proof for the different reactivities observed between the molybdenum oxide and tungsten oxide clusters.[88,89]

However, thus far, the roles played by a plethora of significant factors in the liberation of H_2 from water using cluster models of TMOs, viz., the different types of oxygen vacancies on different metal oxide surfaces, the differing metal−oxygen and metal−hydrogen bond strengths, the initial electrostatic complexes formed, the geometric factors involved, the mechanistic aspects associated with using slightly bigger clusters to better mimic the bulk metal oxide surface, and the loss of entropy when water and the TMO cluster react remain poorly understood. It is therefore critical to deeply examine these facets.

This comprehensive work provides new insights on all of these crucial aspects. On the basis of previous experimental

Received: July 24, 2013
Published: October 10, 2013

dx.doi.org/10.1021/ja4076309 | J. Am. Chem. Soc. 2013, 135, 17039−17051

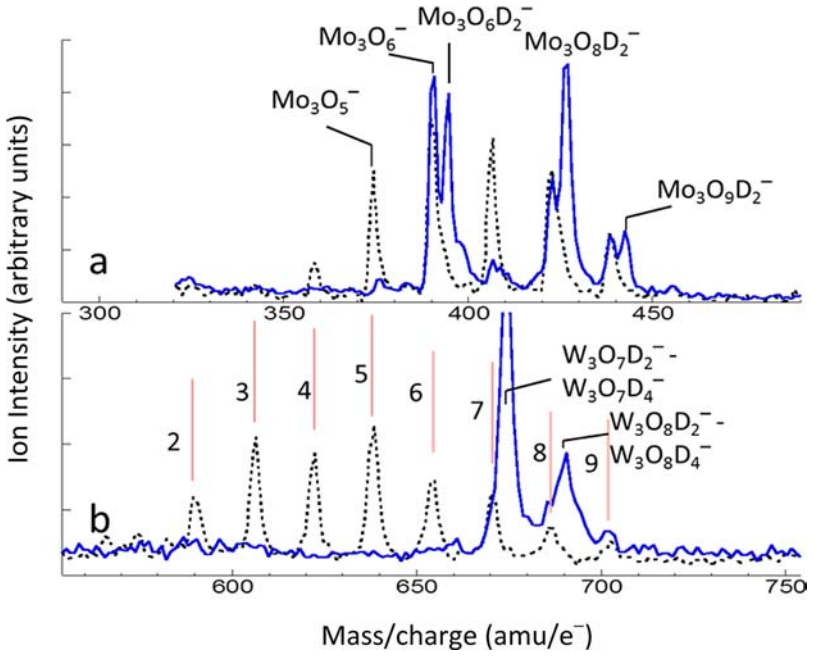

Figure 1. Mass spectra of (a) $Mo_3O_y^-$ and (b) $W_3O_y^-$ clusters prior to exposure to D_2O (dotted traces) and after exposure to D_2O (solid blue traces).[89]

work[89] and using additional photoelectron spectroscopic data in the present work, we computationally explain why the disparity noticed in the chemical reactions of $W_3O_5^-$ and $Mo_3O_5^-$ clusters with H_2O exists. This is a notably challenging problem as the ground states of $W_3O_5^-$ and $Mo_3O_5^-$ have nearly identical molecular and electronic structures (C_s symmetric geometries and doublet spin multiplicities). Consequently, very similar reactivity patterns are expected for both the metal oxides, and a multitude of reaction pathways need to be carefully screened to detect any difference that can profoundly impact the net reactivities.

The $Mo_3O_6H_2^-$ kinetic trap formed in the reaction of $Mo_3O_5^-$ with water can potentially be attributed to several different kinds of structures. We demonstrate our novel observation that out of various possibilities a specific dihydroxide structure can be assigned. In the case of $W_3O_5^-$ getting oxidized to $W_3O_6^-$ and releasing H_2, we suggest that the geometry of the $W_3O_6^-$ obtained after oxidation is the same as the lowest-energy isomer of $W_3O_6^-$.

Our proposed mechanistic rationale for these interesting questions—(a) why does the molybdenum oxide form a kinetic trap? (b) what is the chemical structure of the kinetic trap? (c) why does the molybdenum oxide not get oxidized to liberate H_2? (d) why does the tungsten oxide get oxidized to liberate H_2 (and not form a kinetic trap instead)? (e) is the oxidized product the lowest-energy isomer?—offers valuable lessons on the salient factors governing the generation of H_2 from water.

EXPERIMENTAL DETAILS

The experimental apparatus used in this study has been described in detail elsewhere.[25,90] Briefly, $^{98}Mo_3O_6H_2^-$ or $^{98}Mo_3O_6D_2^-$ complexes are generated by reactions between $^{98}Mo_xO_y^-$ cluster anions and H_2O or D_2O in a high-pressure, fast flow reactor coupled to a laser ablation/pulsed molecular beam source similar to that developed by Dietz and co-workers.[91] Approximately, 10 mJ/pulse of the second harmonic (532 nm) output of a Nd:YAG laser is focused onto a rotating ^{98}Mo disk target (Oak Ridge National Laboratory, Isotope Business Office). The resulting plasma is entrained in a pulse of ultra-high-purity helium gas delivered from a solenoid-type molecular beam valve (40 psig backing pressure) to facilitate cluster formation and cooling. The cluster/He mixture then flows into 2.5 cm long, 0.3 cm diameter clustering channel into which a second pulsed valve injects H_2O or D_2O (Sigma Aldrich, 99.9 atom % D) at ambient vapor pressure at room temperature (3125 Pa, or 0.46 psi at STP), seeded into He (40 psig backing pressure). The increased chemical potential resulting from pressure >10^5 Pa does increase the water vapor pressure but only on the order of 1%.

The resulting products expand into a vacuum chamber, pass through a 3 mm skimmer, and the negatively charged species are accelerated on axis into a 1.2 m beam-modulated time-of-flight mass spectrometer. After passing through the 3 mm mass defining slit, the ions travel another 80 cm before colliding with a dual microchannel plate detector assembly. At 15 cm upstream of the ion detector, negative ions are photodetached using the third harmonic output (3.49 eV, 355 nm) of a second Nd:YAG laser timed to individually intersect only the ions of interest. The few photoelectrons that travel the length of a 1 m field-free drift tube situated perpendicular to the ion beam axis are detected with a microchannel plate detector assembly at the end of the drift tube, and their flight times are recorded using a digitizing oscilloscope. The drift times are converted to kinetic energy (e^-KE) and subsequently to electron binding energy (eBE = $h\nu$ − e^-KE), calibrated using the well-known spectra of I^-, O^-, OH^-, and WO_2.[92] The spectra shown here were collected for approximately 500 000−1 000 000 laser shots.

COMPUTATIONAL DETAILS

The Gaussian suite of programs has been used for all our calculations.[93] The optimized geometries and single-point energies of all the species were obtained with the unrestricted version of the B3LYP[94,95] hybrid density functional. The 60 core electrons of tungsten and 28 core electrons of molybdenum were replaced with the Stuttgart−Dresden relativistic pseudopotentials.[96] The remaining 14 valence electrons on both these metal centers were treated with an augmented version of the associated double-ζ basis sets including diffuse and polarization functions.[96] Double-ζ quality contracted 9s5p Gaussian functions (also informally known as the D95 basis set) including additional diffuse and polarization functions were used to treat H and O.[97] Vibrational analyses have been carried out to confirm the nature of all the minimum energy structures and transition states.

dx.doi.org/10.1021/ja4076309 | J. Am. Chem. Soc. 2013, 135, 17039−17051

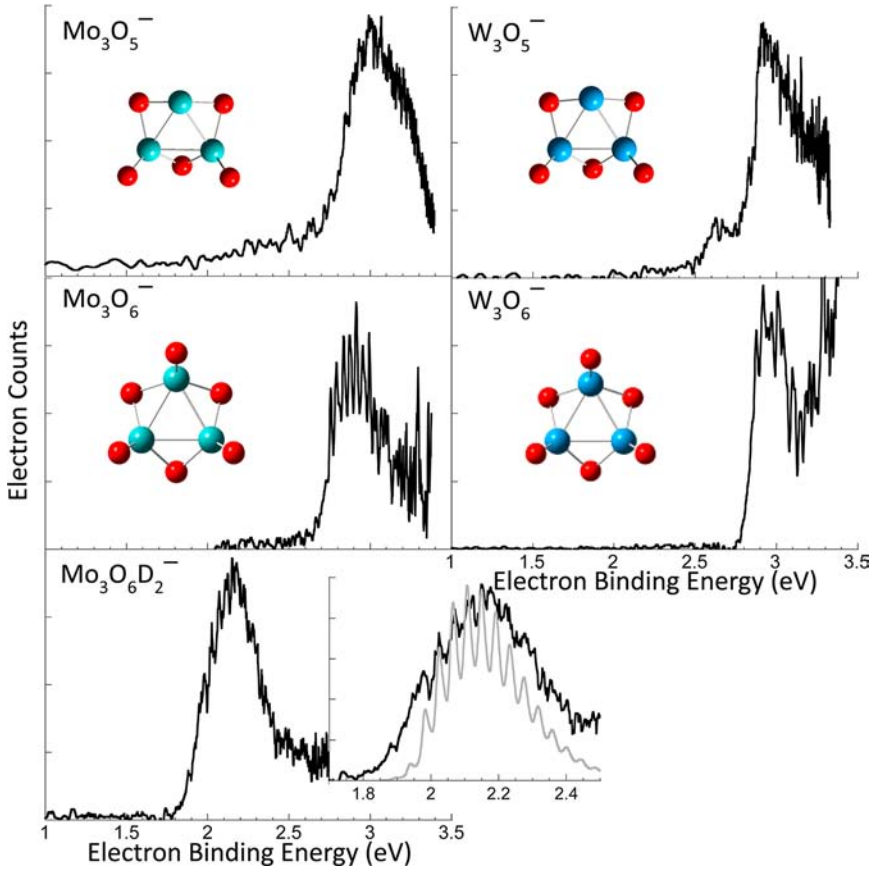

Figure 2. PE spectra of $Mo_3O_5^-$, $Mo_3O_6^-$, and the tungsten analogues,[67] along with the PE spectrum of $Mo_3O_6D_2^-$, for which there is no tungsten analogue. The inset shows the PE spectrum of $Mo_3O_6D_2^-$ on an expanded scale, with the PE spectrum of $Mo_3O_6^-$ superimposed and shifted to lower binding energy to illustrate the similar vibrational spacings.

The resulting zero-point energies and thermal corrections have been included in all the free energies obtained. Intrinsic reaction coordinate (IRC) calculations were carried out to verify that key transition states connect to the minima on either side.

The effects of larger basis sets on the computed reaction energies were then evaluated by single-point calculations using larger augmented triple-ζ basis sets. The aug-cc-pVTZ[98] basis set was used to treat H and O. The same pseudopotential/basis set combination as described in the previous paragraph (Stuttgart−Dresden relativistic pseudopotential) was used for the metal centers (Mo and W) but two extra f-type functions and a g-type function were added to the basis set. The additional exponents used in both the double-ζ and the triple-ζ quality basis sets are provided in the Supporting Information. Finally, a small additional correction to barrier heights based on the M06 functional has been added to all the transition states described in the main text involving hydrogen migration as a radical, that is, for those transition states involving (a) a hydrogen transfer from oxygen to metal and (b) hydrogen liberation. This correction is based on the identification of a deficiency for the B3LYP functional for such transition states and a careful calibration of the systematic errors on the associated energy barriers. It is related to the low barrier predicted by B3LYP for the H + H_2 or F + H_2 reactions that is manifested to different extents in different molecules. We calibrated the magnitude of this error for hydrogen atom migration in Mo and W oxides by comparison with the M06 functional[99] and found that the underestimation of the barrier is about 3 kcal/mol. This correction factor is typically smaller than the differences in the barrier height (which is roughly about 7−8 kcal/mol in this study) between the Mo oxide and W oxide clusters. Furthermore, since the same correction is applied to both the Mo oxide and W oxide clusters, it does not affect the relative energy barriers between the two families of reactions. In most of the other reactions considered in this study, the barriers obtained by B3LYP and M06 are very similar.

RESULTS AND DISCUSSION

Experimental PE Spectrum of $Mo_3O_6D_2^-$. As was reported previously,[89] the product distribution of reactions between the trimetallic $Mo_3O_y^-$ oxide series and water (H_2O or D_2O) exhibits striking differences from the product distribution observed in $W_3O_y^-$ + water reactions, which is summarized in Figure 1. Of particular note is that the $Mo_3O_6D_2^-$ product seen in Figure 1a has no analogue in the $W_3O_y^-$ + D_2O reaction product distribution, shown in Figure 1b. Analogous results were obtained in studies on H_2O reactions; results of the D_2O studies are shown here because the ion signals from $M_3O_y^-$ and $M_3O_yD_2^-$ are more clearly resolved.

Figure 2 shows the PE spectrum of $Mo_3O_6D_2^-$ (bottom panel, obtained in this work), along with the previously obtained PE spectra of $Mo_3O_5^-$ and $Mo_3O_6^-$ and the respective tungsten analogues (top two panels).[67] Also included are the lowest-energy structures calculated for the anions ($Mo_3O_5^-$, $Mo_3O_6^-$, the corresponding tungsten analogues,[67] and $Mo_3O_6D_2^-$), all of which yield results that are in excellent agreement with the observed spectra.

The PE spectrum of $Mo_3O_6D_2^-$ is very similar in profile to the PE spectrum of $Mo_3O_6^-$ both in terms of the observed vibrational spacing, 340 cm^{-1} (which corresponds to a ring-breathing mode of $Mo_3O_6^-$), and the overall width of the electronic transition. The adiabatic electron affinity (EA_a) of $Mo_3O_6D_2^-$, which corresponds to the origin of the electronic

dx.doi.org/10.1021/ja4076309 | J. Am. Chem. Soc. 2013, 135, 17039−17051

detachment transition, or adiabatic detachment energy (ADE), is 1.984(40) eV; the large uncertainty is due to the difficulty in identifying the origin peak of an extended progression.[100] To underscore the similarity between the $Mo_3O_6D_2^-$ and $Mo_3O_6^-$ spectra, the computation-based simulation of the latter, shifted 0.770 eV to lower eBE, is superimposed on the experimental spectrum of the former and shown on an expanded eBE scale as an inset in Figure 2. Observation of this partially resolved low-frequency progression argues against the presence of any labile hydroxyls in the complex, which would significantly broaden the transition because of nearly free rotation of the hydroxyl group, the orientation of which would be affected greatly by a change in charge state of the complex and suggests the presence of a single isomer.

Computational Results and Analysis. The ground-state geometries of both $W_3O_5^-$ and $Mo_3O_5^-$ are predicted to have doublet electronic states. These clusters contain three bridging metal−oxygen bonds and two terminal metal−oxygen bonds. They are reminiscent of the symmetric C_{3v} structures seen previously[56] for $W_3O_6^-$ and $Mo_3O_6^-$, but with an oxygen vacancy on one metal center in each of these clusters (Figure 3). The reacting water molecule can form several electrostatic complexes with the metal oxides depending on the different possible ways in which water can approach the clusters. Each of these complexes can then potentially lead to different reaction pathways.

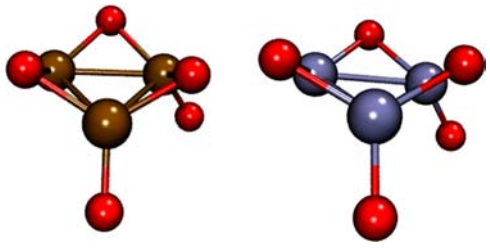

Figure 3. Lowest-energy isomers of the doublet electronic states of $Mo_3O_5^-$ (left) and $W_3O_5^-$ (right). Other orientations more easily represent their C_s symmetry, and a top-down view is provided in the Supporting Information.

In the following discussion, we shall first explore the electrostatic complexes, followed by ascertaining the chemical structure of the kinetic trap formed in the reaction of $Mo_3O_5^-$ with water. Subsequently, the pathway leading to H_2 liberation in the $W_3O_5^- + H_2O \rightarrow W_3O_6^- + H_2$ reaction is discussed. Then, we draw insights from the processes that do not occur, such as kinetic trap formation in the reaction of $W_3O_5^-$ with water and H_2 liberation in the reaction of $Mo_3O_5^-$ with water. Finally, the connection between the cluster models and the bulk surface of the TMOs is made.

This work involves the screening of an exhaustively large number of reaction energy pathways. Therefore, to help the reader focus on the major points, we present all the peripheral reaction pathways (which nonetheless provide important details that help us in reaching our conclusions) in the Supporting Information and enunciate only the major pathways in the main text.

(a). Initially Formed Electrostatic Complexes. The electrostatic complexes initially formed between water and the cluster anion have profound consequences on further reactivity (vide infra). Figure 4 lists the electrostatic complexes (within 5 kcal/mol of the most stable complex) in order of increasing relative free energies. With both molybdenum and tungsten oxide, the most favorable approach is when the oxygen of water is aligned toward the most oxidized metal center (attached to two bridging oxygens and a terminal oxygen).

In the most stable complex, **C1**, the two hydrogens point toward the two bridging oxygens. Complex **C2**, in which the hydrogens point toward the two terminal oxygens in the clusters, is almost as stable as **C1**. In **C3** and **C4**, both resulting via the sideways approach of water, only one hydrogen is aligned toward a bridging oxygen in the clusters. The only

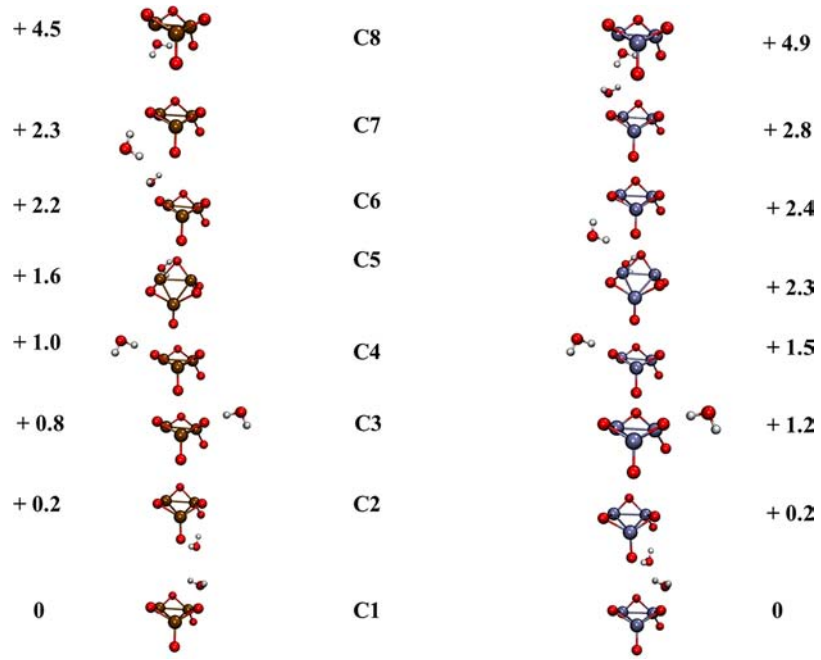

Figure 4. Different electrostatic complexes formed in the initial complexation of water with $Mo_3O_5^-$ (left) and $W_3O_5^-$ (right) ordered in terms of increasing free energy (kcal/mol).

dx.doi.org/10.1021/ja4076309 | J. Am. Chem. Soc. 2013, 135, 17039−17051

difference between **C3** and **C4** is that, in **C3**, water complexation occurs along the side containing the more oxidized center, whereas in **C4**, water approaches the cluster from the other side, that is, along the side containing the less oxidized metal center.

Complex **C5** is formed when the oxygen of water is oriented toward the less oxidized metal, wherein one hydrogen of water aligns itself along a bridging oxygen of the cluster. While the energy ordering of the first five complexes is the same for $Mo_3O_5^-$ and $W_3O_5^-$, there is a reversal in the ordering for the next two complexes. **C6** for $Mo_3O_5^-$ occurs via water complexation from the top face such that both the hydrogens of water are aligned toward two bridging oxygens. In **C7**, complexation takes place sideways with the hydrogens of water being hydrogen bonded to one terminal and one bridging oxygen. For $W_3O_5^-$, this order is reversed; that is, **C6** is formed via sideways complexation and **C7** from the top. Finally, complex **C8**, in which water attaches to the metal oxides from the bottom face, has one hydrogen pointing toward a terminal oxygen of the metal oxide and the water oxygen aligning toward the less oxidized metal.

The entire relative free-energy window (Figure 4) for these complexes spans 5 kcal/mol. A more detailed thermodynamic analysis of the electrostatic complexes breaking up the free-energy component into the enthalpy part and the entropy part and the effects of including Grimme's empirical D3 dispersion corrections with two different damping functions[101] are given in the Supporting Information.

Table 1 lists the Boltzmann weighted population of all these complexes **C1**−**C8** at room temperature. In the case of both the Mo oxide as well as the W oxide, lower-energy complexes **C1**−**C4** predominate and higher-energy complexes **C5**−**C8** contribute less than 10%. It is, however, interesting to note that even though **C8** is about 5 kcal/mol higher on the free-energy scale with respect to the most stable complex **C1**, it (**C8**) can be readily obtained from **C2** (Figure 5). This ready interconvertibility between **C2** and **C8** thus provides access to a higher-energy complex which does not have a significant initial population and has major implications for further reactivity (vide infra).

Table 1. Listing the Boltzmann Weighted Population of Electrostatic Complexes C1−C8 Formed in the Reaction of Water with Mo Oxide and W Oxide Clusters

population for Mo oxide (%)	complex	population for W oxide (%)
0.4	C8	0.3
3.3	C7	2.4
3.6	C6	3.5
6.4	C5	3.6
12.1	C4	8.5
15.5	C3	11.7
26.6	C2	31.0
32.1	C1	39.0

(b). Kinetic Trap Formed with $Mo_3O_5^-$. The experimental PES for $Mo_3O_6D_2^-$ (Figure 2, bottom panel), formed when $Mo_3O_5^-$ reacts with water, is suggestive of a unique, symmetric structure with a neutral EA_a of 1.984(40) eV and a vertical detachment energy (VDE) of 2.16(2) eV. We postulate the existence of a unique symmetric structure given that we were able to resolve the vibrational structure in spite of the expectation that the hydroxyl groups would broaden and blur the features.

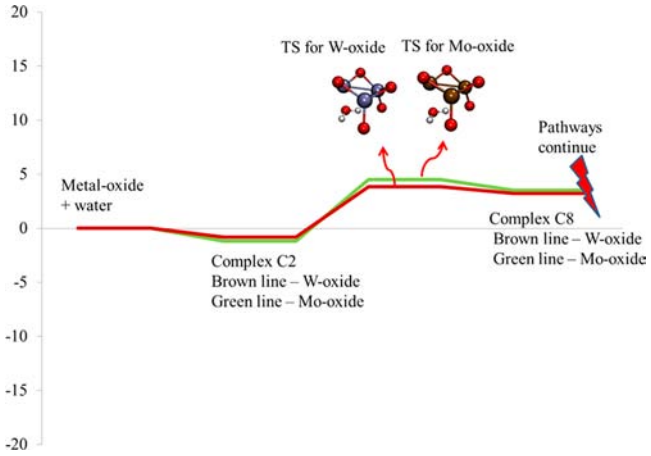

Figure 5. Interconversion between complexes **C2** and **C8**. *Y*-axis is in terms of free energy (kcal/mol). The Supporting Information provides a comparison between the free energies and enthalpies for all the intermediates and transition states.

A priori, the kinetic trap can correspond to (a) dihydridic structures, (b) hydride−hydroxide structures, or (c) dihydroxide structures.

Computations indicate that different dihydridic structures, in which the two hydrogens are attached to the metal centers, as well as hydride−hydroxide structures, in which one hydrogen is attached to a metal and another to an oxygen, have significantly much higher ADEs and VDEs than those obtained experimentally. Therefore, the dihydridic and hydride−hydroxide structures cannot be the principal products observed experimentally.

Inspection of the cluster geometry reveals that four possible different dihydroxides (Figure 6, **DH1**−**DH4**) are possible, and

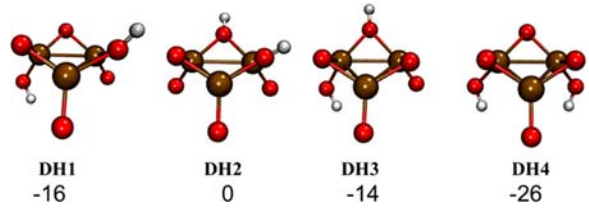

Figure 6. Dihydroxide structures **DH1**−**DH4**, possible structures for the kinetic trap formed in the reaction of $Mo_3O_5^-$ with water. The numbers under the labels are the relative free energies (kcal/mol) for the dihydroxides.

the computed ADE/VDEs for all four of these dihydroxides are similar and in good agreement with the experimentally obtained ADE/VDE values (1.98/2.16 eV, vide supra).

While all four structures have a common symmetric framework consisting of three bridging and three terminal oxygens, as in the core framework of the lowest-energy isomer of $Mo_3O_6^-$,[67] they differ in the position and the relative orientations of the two OH groups with respect to each other.

In **DH1**, one OH group is a bridging hydroxyl group and the other is a terminal hydroxyl group on the opposite side. **DH2** has both the OH groups positioned as bridging hydroxyl groups. Similar to **DH1**, **DH3** has a bridging hydroxyl group and a terminal hydroxyl group, but here, both the OH groups are adjacent to one another. Finally, in **DH4**, both the hydroxyl

dx.doi.org/10.1021/ja4076309 | J. Am. Chem. Soc. 2013, 135, 17039−17051

groups are terminal OH groups. Among all of these dihydroxides, **DH4** is the most stable one.

We systematically begin with the lowest-energy molybdenum oxide−water complex **C1** and trace out the pathways that lead to further chemical reactions. An apt starting point is via the "fluxionality pathway", which involves a series of proton hops that sample various possibilities when multiple potential pathways exist.[56,57]

C1 results in the dihydroxide **DH1** (Figure SI_1). However, we rule out its formation since it involves a 15 kcal/mol free-energy barrier in the third step—which is a high enough barrier at the experimental room temperature conditions in the gas phase. Moreover, **DH1**, if formed, will be readily converted into a hydridic intermediate (step 7, Figure SI_1) that happens to be a thermodynamic sink. Thus, any pathway leading to **DH1** will result in this hydridic intermediate that is not consistent with the experimentally observed detachment energies. Therefore, **DH1** can be ruled out as the kinetic trap.

We observe that complexes **C2**, **C3**, **C4**, and **C7** (Figure 4) do not lead to any productive reaction pathways *directly*. In each of these complexes, the orientation and/or the distances of the oxygen and hydrogens are not optimal with respect to the reactive sites in $Mo_3O_5^-$ to favor chemical bond formation. In the case of **C2**, whereas the hydrogens can readily bond with the terminal oxygens in the cluster, the oxygen of water is too far from any electropositive metal center. In both **C3** and **C4**, one hydrogen of water is in close proximity to a bridging oxygen in the clusters, but the other OH group of water is not appropriately placed for further chemical reactivity. Similarly, in **C7**, the oxygen atom of water is unfavorably positioned to lead to subsequent reactions.

Complex **C5**, however, can participate in chemical bond formation and leads to the formation of **DH3** (Figure SI_2). Starting with $Mo_3O_5^-$ and water, the formation of **C5** does not occur with any significant stabilization or destabilization on the free-energy scale (step 1, Figure SI_2). Following water dissociation in step 2 (Figure SI_2), which proceeds with a 3 kcal/mol barrier, we obtain an asymmetric dihydroxide intermediate (Figure SI_2). Given the unfavorable distances and the relative orientation of the reactive sites within this asymmetric dihydroxide, further proton hop[56,57] is not feasible. Interestingly, however, the newly formed Mo−OH bond in step 2 undergoes a barrierless rotation to yield **DH3** (Figure SI_2), which is 15 kcal/mol more stable than the reactants.

Similarly, complex **C6** also results in **DH3** (Figure SI_3).[102] Initially, **C6** is free-energetically slightly destabilized with respect to the reactants by just about 1 kcal/mol (step 1, Figure SI_3). Then, water in **C6** is positioned very favorably with respect to $Mo_3O_5^-$ for a facile fluxionality pathway[56,57] to occur. Indeed, the formation of the intermediate in step 2 with a 5 kcal/mol free-energy barrier (Figure SI_3) mirrors the fluxionality pathway. At this stage, the Mo−OH bond in step 2 (Figure SI_3) readily rotates without any barrier (step 3, Figure SI_3). This pathway results in the same asymmetric dihydroxide intermediate (herein, as well, we actually get the mirror image, but we do not make a distinction; see ref 102) formed in step 2 in Figure SI_2. The pathways from complexes **C5** and **C6** converge here,[102] and **DH3** is finally obtained in step 4 (Figure SI_3).

Interestingly, although **C2** directly does lead to further chemical reactivity, it gets readily converted to **C8** (Figure 5). From **C8**, direct dissociation of water with a 6 kcal/mol free-energy barrier results in the formation of the C_s symmetric **DH4** as seen in Figure 7. This pathway results in the most stable $^2A''$ electronic state of **DH4** (Figure 7 and Figure 9, vide infra). It is necessary to recognize here that the 6 kcal/mol free-energy barrier largely arises from the entropic component of two species (TMO cluster and water) coming together to form a single complex at the very beginning.

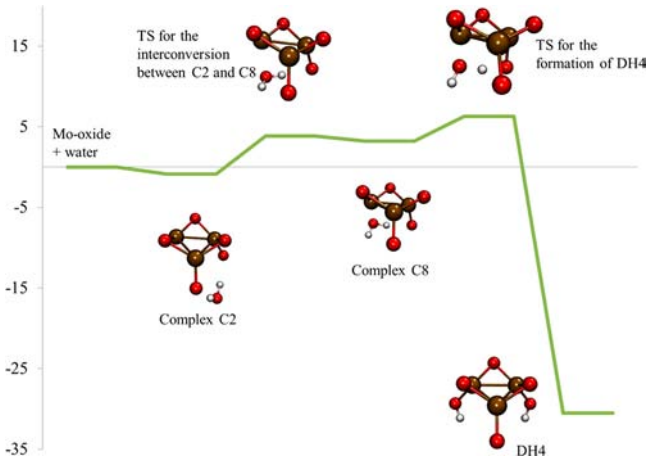

Figure 7. Reaction pathways (*Y*-axis is in terms of free energies, kcal/mol) for the formation of the kinetic trap **DH4** starting from complex **C2** via **C8**. The Supporting Information provides a comparison between the free energies and enthalpies for all the intermediates and transition states.

Thus far, we have facile pathways that lead to the formation of dihydroxides **DH3** and **DH4**. Whereas **DH3** is the kinetically favored product (with a highest barrier of only 3 kcal/mol, Figure SI_2), **DH4** is the thermodynamically most favored product and is overwhelmingly more stable than **DH3** by 10−11 kcal/mol. In addition, relative to the formation of **DH3**, the barrier for the formation of **DH4** involves only a small additional energy of 3 kcal/mol (with a net barrier of 6 kcal/mol, Figure 7). Hence, it is very likely that thermodynamically favored product is readily accessible.

Additionally, the formation of **DH4** occurs through the electrostatic complex **C8**, which in turn is readily accessible from the significantly populated electrostatic complex **C2** (Table 1). In contrast, **DH3** is obtained from the higher-energy complexes **C5** and **C6** which are sparsely populated. Therefore, thermodynamic arguments clearly support the formation of **DH4** over **DH3**.

Further support for assigning the observed $Mo_3O_6H_2^-$ structure to **DH4** arises from the simulated PES generated using calculated spectroscopic parameters, including the computed values for ADE (1.93 eV), the VDE (2.23 eV), and the predicted activity of the vibrational modes based on normal coordinate displacements. The computed ADE and VDE values are in excellent agreement with the observed values, 1.984(40) and 2.16(2) eV, respectively, and the most active mode in the spectrum is a 287 cm^{-1} neutral ring distortion mode which results in the overall profile of the electronic transition. Spectral simulations generated using the PESCAL code[103] assuming anion vibrational temperatures of both 300 and 500 K are shown in Figure 8 and suggest that the complex anion temperature is above room temperature but below 500 K. This is consistent with (a) the internal energy gained from addition of water to the cluster anion resulting in the formation of **DH4** and (b) insufficient internal energy to

dx.doi.org/10.1021/ja4076309 | J. Am. Chem. Soc. 2013, 135, 17039−17051

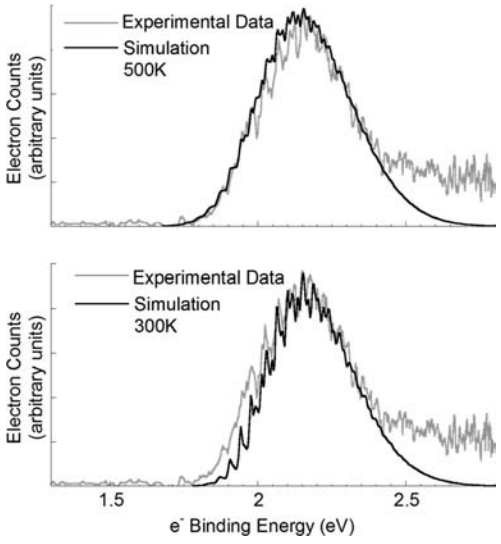

Figure 8. Simulated PES spectrum of **DH4** being compared with the experimentally obtained PES at 500 and 300 K, supporting the formation of **DH4**.

overcome the calculated barrier for **DH4** to react further (vide infra).

A complete list of the neutral vibrational modes that are predicted to be active in the transition, the corresponding anion frequencies, the Cartesian normal coordinate displacements calculated using the FCFGauss code,[104] transition origin, and peak widths are included in the Supporting Information. It should be noted that simulations using spectroscopic parameters calculated for the alternative dihydroxide structures were comparable to the simulations shown in Figure 8, though the overall width of the alternative simulations is less consistent with observed spectrum, and the most active modes did not match as well with the observed progression. Therefore, while **DH1**, **DH2**, and **DH3** could not be definitively eliminated based on PES simulations alone, they were overall notably less consistent with the observed spectrum.

Based on these results, the similarity between the PE spectra of $Mo_3O_6^-$ and $Mo_3O_6D_2^-$ appears to be somewhat coincidental. In the case of $Mo_3O_6^-$,[105] the HOMO of the anion, which is the orbital associated with the detachment transition, was previously found[105] to be a_1 symmetrically delocalized over all three metal centers. The **DH4** structure has two additional electrons in the Mo-based orbitals, and the HOMO, shown in Figure 9, correlates to one of the "e" degenerate LUMOs of $Mo_3O_6^-$. However, in both cases, detachment from the Mo-based orbitals results in activation of ring distortion modes with similar frequencies.

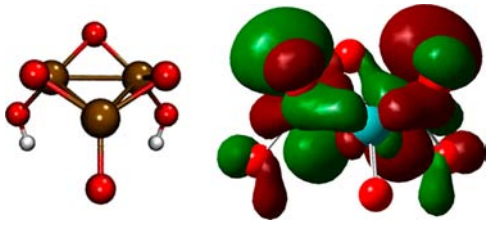

Figure 9. Dihydroxide **DH4**, the kinetic trap formed in the reaction of $Mo_3O_5^-$ with water and its HOMO. For the sake of clarity, the orientation of the atoms is maintained in the ball and stick representation as well as the HOMO.

(c). H_2 Liberation Pathway with $W_3O_5^-$. Experimental mass spectrometric evidence suggests that, upon reacting with water, $W_3O_5^-$ gets oxidized to $W_3O_6^-$. This process is accompanied with the release of molecular hydrogen. It is unclear from the experimental PES whether the lowest-energy isomer of $W_3O_6^-$ is formed or an isomer different from the lowest-energy isomer of $W_3O_6^-$ is formed in the process. Therefore, in addition to finding an appropriate pathway for H_2 liberation, we also need to ascertain the structure of the oxidized product formed.

As an initial guideline, we use our knowledge[88] that the generation of molecular hydrogen in the reaction of TMOs with water requires that suitable sites bearing a hydridic hydrogen (i.e., a metal−hydrogen bond) and a protonic hydrogen (i.e., a metal−hydroxide bond) be created in the TMOs. In concurrence with this guideline, we were unable to find low-energy pathways to release H_2 from a dihydridic or a dihydroxide structure. Our strategy to obtain the most favorable H_2 liberation pathway therefore focuses on suitably obtaining a hydride−hydroxide intermediate and figuring out the most profitable way of oxidizing the metal oxide cluster thereupon.

As with the molybdenum oxide (vide supra), we start with the lowest-energy complex **C1** obtained when $W_3O_5^-$ reacts with water. Steps 1−5 in Figure SI_4 are in accordance with the fluxionality pathway,[56,57] that is, complexation (step 1) followed by the formation of an initial adduct (step 2), opening up of a bridged oxygen (step 3), proton hop (step 4), and finally the re-formation of a bridging oxygen (step 5) overall leading to the dihydroxide intermediate obtained at step 5. Of these, steps 3 and 5 are the rate-determining steps with barriers of about 11 kcal/mol on the free-energy scale. In step 6, with a barrier of about 10 kcal/mol, a hydride−hydroxide intermediate (**HHI**) which has a metal−hydrogen bond and a metal−hydroxyl bond is formed. The remaining mechanistic steps are all downhill to eventually form a higher-energy isomer of $W_3O_6^-$ (Figure SI_4). A related pathway (Figure SI_5), branching out in step 7 from the pathway in Figure SI_4, results in the formation of the lowest-energy isomer of $W_3O_6^-$. However, since both of these pathways involve significant barriers of 10−11 kcal/mol, we look for pathways with lower barriers.

We notice that complex **C2**, via **C8**, provides two such pathways. For the W oxide, once the higher-energy complex **C8** is accessed (via **C2**, brown line, Figure 4), it can further lead to the formation of a diydroxide intermediate (first step in Figure 10 and Figure 11) with a free-energy barrier of 6 kcal/mol. As discussed previously in the case of the Mo oxide forming the kinetic trap, the barrier herein as well arises from an entropic penalty. The dihydroxide which is about 32−33 kcal/mol more stable relative to the reactants on the free-energy scale now has two different pathways to lead to hydrogen liberation without any barrier at all.

In the first pathway (Figure 10), the hydrogen from an OH group hops over from an oxygen to a tungsten center (second step, Figure 10) from the bottom face, that is, along the same face as the terminal oxygens, to form a hydride−hydroxide intermediate (**HHI**). This **HHI** very readily loses hydrogen to result in the oxidation of $W_3O_5^-$ forming the lowest-energy isomer of $W_3O_6^-$.

In the second, somewhat more complicated route (Figure 11), an OH group hydrogen undergoes a successive series of fluxionality steps to result in a different **HHI** (eventually

dx.doi.org/10.1021/ja4076309 | J. Am. Chem. Soc. 2013, 135, 17039−17051

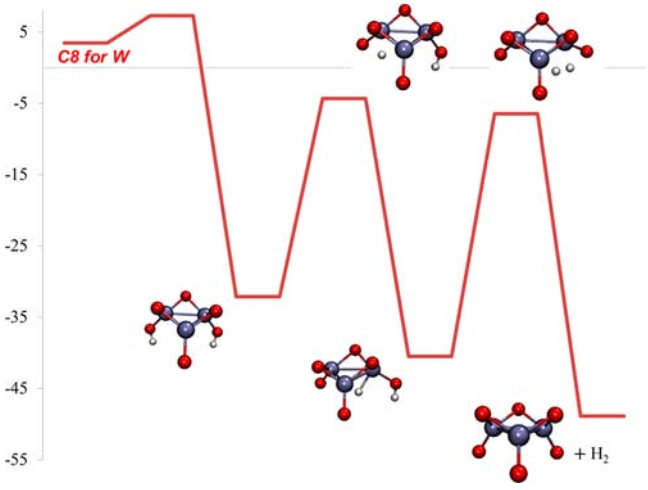

Figure 10. Reaction pathways (*Y*-axis is in terms of free energies) for hydrogen liberation in the reaction of $W_3O_5^-$ with water at 298 K. For ease of comprehension, only the key steps are shown. The Supporting Information provides a comparison between the free energies and enthalpies for all the intermediates and transition states.

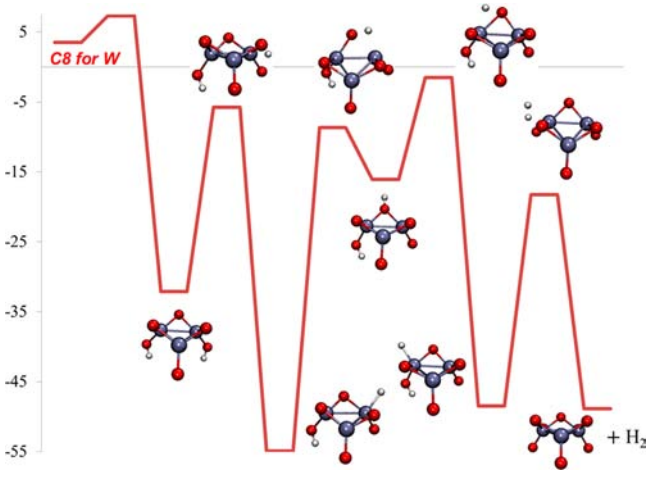

Figure 11. Another reaction pathway (*Y*-axis is in terms of free energies, kcal/mol) for hydrogen liberation in the reaction of $W_3O_5^-$ with water at 298 K. For ease of comprehension, only the key steps are shown, starting with complex **C8** for the W oxide. A more detailed picture, including all the other insignificant steps such as minor bond rotations which do not alter the science in anyway, is shown in the Supporting Information. The Supporting Information also provides a comparison between the free energies and enthalpies for all the intermediates and transition states.

formed in the fourth step, Figure 11) that eliminates hydrogen. The key difference between the **HHI**s formed in Figures 10 and 11 is that the **HHI** in Figure 10 has both the metal–hydrogen bond and the metal–hydroxyl bond in the bottom face, whereas the **HHI**s formed in Figure 11 have the metal–hydrogen bond in the top face and the metal–hydroxyl bond in the bottom face. The net essence is that, in our case, irrespective of the relative orientation of the metal–hydrogen and metal–hydroxyl bonds, a barrierless hydrogen liberation ensues.

Besides **C1** and **C2** (via **C8**), the only other tungsten oxide–water complex which can directly result in a H_2 liberation pathway is **C7**. Starting with **C7**, an **HHI** can be obtained by starting with a fluxionality pathway (Figure SI_6 in Supporting Information), and the **HHI** can subsequently lead to H_2 elimination (as seen in steps 6–8 in Figure SI_4). However, two initial steps involve 11 and 21 kcal/mol barriers. Therefore, the pathway starting with **C7** is readily ruled out. Further, based on the same reasons as with the molybdenum oxide–water complexes (vide supra), other tungsten oxide–water complexes such as **C3** and **C4** do not directly engage in any productive chemical reaction pathways. Even if any kinetic traps are formed (Figures 10, 11, SI_7, and SI_8), they go on to lead to hydrogen liberation.

Hence, out of the five pathways resulting in hydrogen liberation (Figures SI_4, SI_5, SI_6, 10, and 11), the pathways starting with **C8** (which is in turn obtained from **C2**) are the most favorable with a 6 kcal/mol barrier involved (Figures 10 and 11), leading to H_2 liberation as well as the formation of the lowest-energy isomer of $W_3O_6^-$.

(d). Non-Occurring Processes. So far, we have satisfactorily explained the processes that occur, that is, the formation of a kinetic trap in the reaction of molybdenum oxide with water and the liberation of H_2 with the tungsten oxide in the reaction $W_3O_5^- + H_2O \rightarrow W_3O_6^- + H_2$. However, a complete picture emerges only when we fully understand the processes that do not occur.

We first consider the question of why $Mo_3O_5^- + H_2O$ does not yield $Mo_3O_6^- + H_2$. There are two approaches to answer this question. The first approach involves tracking the intermediate **DH4** and evaluating whether **DH4** can react further to liberate H_2. In the second approach, other pathways starting from $Mo_3O_5^-$ need to be explored for hydrogen liberation pathways.

Beginning with the first approach, we track the possible reaction pathways from **DH4** leading to hydrogen liberation and directly compare the hydrogen liberation pathways for Mo oxide and W oxide in Figures 12 and 13 (also see Figures SI_9 and SI_10). The steps involved with both the TMOs are identical. *Yet, subtle but important differences in the relative barrier heights are noted.* For the Mo oxide, **DH4** is stabilized by 30 kcal/mol with respect to the reactants, comparable to a similar stabilization of 32 kcal/mol for the W oxide analogue. Under collision-free conditions, this energy is still available for subsequent reorganizations or reactions. In the case of Mo oxide, for subsequent reactivity leading to H_2 liberation, **DH4** has to cross a barrier of about 33–35 kcal/mol, thus exceeding the 30 kcal/mol free energy gained in its formation (top part of Figures 12 and 13). While this suggests a low probability for H_2 liberation, any energy lost in collisions will decrease it further. Additionally, the short residence time in the experimental ion chamber will also decrease the probability of H_2 liberation within the time scale of the experiment due to kinetic shift.[106] In contrast, the analogous barrier associated with the tungsten analogue of **DH4** is only about 28 kcal/mol, well below the 32 kcal/mol free energy gained as a result of its formation.

As part of the second approach, after an exhaustive search, we were able to find alternative pathways leading to H_2 liberation from $Mo_3O_5^-$ in its reaction with water from complexes **C6** and **C1**. However, both of them (Figures SI_11 and SI_12; see Supporting Information) contain one or more steps with a very high barrier. When starting with **C1**, step 3 (Figure SI_12, Supporting Information) and step 6 have 19 and 21 kcal/mol barriers, respectively. Similarly, when starting with **C6**, step 3 (Figure SI_11, Supporting Information) has a 23 kcal/mol barrier. All these inaccessible barriers render it impractical for $Mo_3O_5^-$ to lead to molecular hydrogen

dx.doi.org/10.1021/ja4076309 | J. Am. Chem. Soc. 2013, 135, 17039–17051

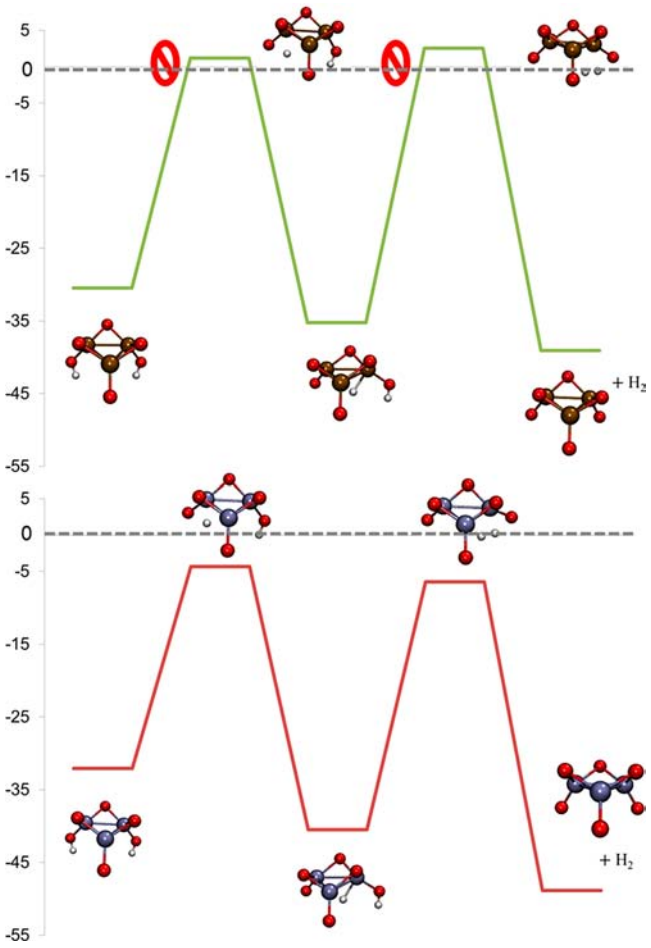

Figure 12. Direct comparison of the key steps in the reaction profiles of W oxide and Mo oxide clusters (top, Figure SI_9 for Mo vs, bottom, Figure 10 for W). *Y*-axis is in terms of free energies (kcal/mol). Once the stable dihydroxide is formed, the W oxide goes all the way without any barrier to liberate hydrogen, whereas the Mo oxide forms a kinetic trap. The Supporting Information provides a comparison between the free energies and enthalpies for all the intermediates and transition states.

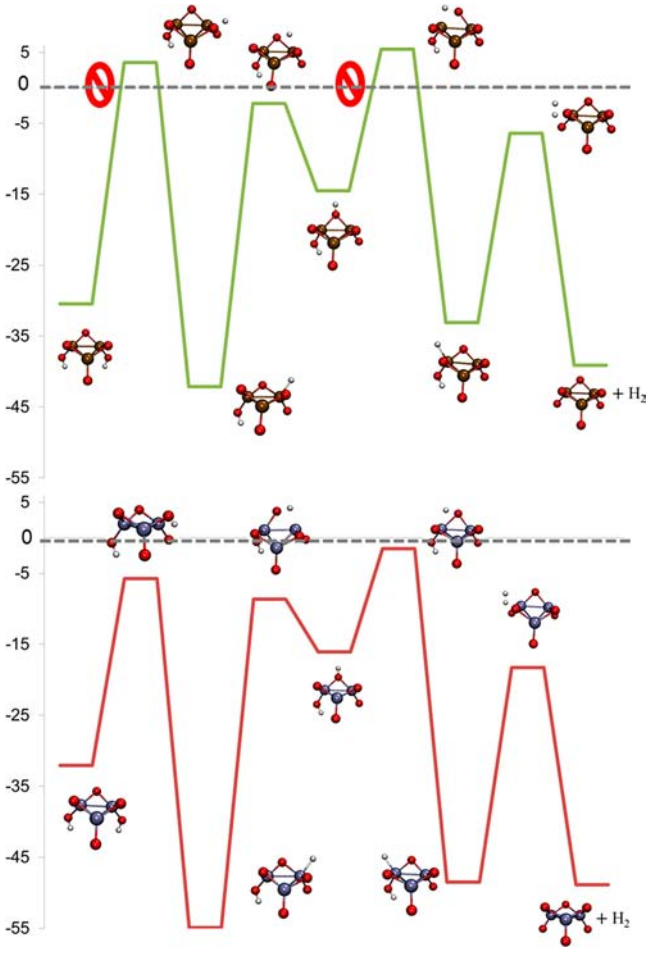

Figure 13. Direct comparison of the key steps in the reaction profiles (top, Figure SI_10 for Mo vs, bottom, Figure 11 for W) of W oxide and Mo oxide clusters. *Y*-axis is in terms of free energies (kcal/mol). Once the stable dihydroxide is formed, the W oxide goes all the way without any barrier to liberate hydrogen, whereas the Mo oxide forms a kinetic trap. The Supporting Information provides a comparison between the free energies and enthalpies for all the intermediates and transition states.

generation, instead leading to the relatively more favorable kinetic trap formation.

The only remaining question now is, why $W_3O_5^-$ does not lead to kinetic trap formation? Figures SI_7, SI_8, 10, and 11 readily answer this question: any kinetic trap that is formed rapidly reacts to liberate hydrogen because barriers lie well below the free energy of the reactants.

It is worthy to note that, in addition to the kinetic limitations, our observation is that the free-energy difference between the final products obtained in the H_2 liberation pathway and the kinetic trap formation pathway is significantly larger for the tungsten oxide (49 − 32 = 17 kcal/mol) than it is for the molybdenum oxide (39 − 30 = 9 kcal/mol). This picture is entirely consistent with the metal−oxygen bond energies reported by Dixon and Peterson.[107] The large difference (17 kcal/mol for the W oxide vs 9 kcal/mol for the Mo oxide) also underscores the enhanced role played by the thermodynamic factors in the case of $W_3O_5^-$ over $Mo_3O_5^-$.

Sections (b) through (d) provide the answers to the questions we sought to answer in the Introduction. *Overall, small differences in the barrier heights are ultimately responsible for the different product distribution noticed between these structurally similar TMOs.*

To establish the accuracy of this work and to determine how sensitive our findings based on these small differences are to the choice of the density functional, we performed additional computations using different density functionals. In particular, we carefully scrutinized whether our qualitative conclusions from Figures 12 and 13 could be reversed. Using the same B3LYP geometries as in Figures 12 and 13, the energies of all the intermediates and the transition states were calculated using three different density functionals M06,[99] ωB97xD,[108] and TPSSh.[109] Throughout, the transition states for the hydrogen transfer from oxygen to metal and hydrogen liberation were uniformly lower in energy by at least 6−8 kcal/mol for $W_3O_5^-$ over $Mo_3O_5^-$. The same qualitative result was arrived at using different geometries (with the M06 functional), as well. Hence, the qualitative conclusions from Figures 12 and 13 are not reversed, and the kinetic trap intermediate formed with the Mo oxide cluster consistently requires a larger barrier (at least 6−8 kcal/mol more) than the W oxide cluster to liberate H_2 even though different density functionals may underestimate the

dx.doi.org/10.1021/ja4076309 | *J. Am. Chem. Soc.* 2013, 135, 17039−17051

barrier heights relative to the reactants (TMO + water) to different extents. Detailed results from these calculations are documented in the Supporting Information.

Interestingly, at the first glance, our overall results appear counterintuitive with respect to the metal−hydrogen bond strengths. The mechanisms we propose for hydrogen liberation involve the cleavage of the metal−hydrogen bonds. In contrast to the experimentally obtained and theoretically supported results in this work, the Mo−H (D_e = 63.3 kcal/mol) and W−H (D_e = 67.8 kcal/mol) bond dissociation energies from the work of Landis and co-workers[110] suggest that the Mo oxide cluster should in fact more readily react further than the W oxide cluster. However, careful analysis readily reveals that while the Mo−H bond may indeed be less stable (and hence prone to be more reactive), *the right intermediate containing the Mo−H bond is kinetically not accessible (Figures 12 and 13) for further reactivity*. This kinetic inaccessibility is due to the consistently larger barriers necessary to reach the intermediates with Mo−H bonds via the transition states that link them to dihydroxides. Overall, the accessibility of the intermediate containing the metal−hydrogen bond is thus more important in this case than the metal−hydrogen bond strengths themselves.

In the coming sections, we connect our cluster models with bulk surfaces and summarize the role played by key factors in the photocatalytic liberation of H_2.

(e). Clusters To Better Model the Bulk Surfaces. Our previous study[88] with small $W_2O_y^-$ (y = 2−6) clusters resulted in barrierless liberation of H_2 for y up to 4. In this study, the use of slightly larger clusters enables us to better mimic the bulk surface. As expected,[111] larger but energetically accessible barriers (6 kcal/mol, Figures 10 and 11) to get H_2 are noticed with $W_3O_5^-$ clusters. Furthermore, similar to the significance of facial and geometric factors typically characteristic of surface reactions, we notice that facial selectivity determines which product is obtained (Figure SI_4 vs Figure 10 or 11). Finally, the free energies for the liberation of H_2 from bulk MO_2 surfaces[112] when they react with water and get oxidized (i.e., in the reactions $MO_2 + H_2O \rightarrow MO_3 + H_2$, M = W or Mo) strongly suggest the favorability of H_2 liberation in the reactions of water with tungsten-oxide clusters over molybdenum-oxide clusters—just as we observe in this study. It is worthwhile to point out here that surface defects can be modeled using both neutral and ionic clusters.[20−22] The results obtained from this study correspond to the anionic clusters $W_3O_5^-$ and $Mo_3O_5^-$. Quantifying the impact of charge on the reactivity of these TMO clusters is an interesting aspect for future exploration.

(f). Key Factors Helpful in Understanding Photocatalytic H_2 Liberation from TMO Surfaces Using Cluster Models. Our detailed study on the reactivity of $W_3O_5^-$ and $Mo_3O_5^-$ clusters with water enables us to enumerate the most important points to be considered when studying the photocatalytic liberation of H_2 using cluster models.

Accessibility of an Intermediate Containing Metal−Hydrogen Bonds versus Metal−Hydrogen Bond Strengths. During the course of a TMO cluster's reaction with water, unless the key intermediate containing a metal−hydrogen bond (such as the HHI in this study) is readily accessed, the metal−hydrogen bonds do not seem to play a major role (vide supra). Therefore, the kinetic accessibility of the right intermediate is an important factor and needs to be attentively studied, especially in cases such as those noticed in this study where the metal−oxygen bond strengths and metal−hydrogen bond strengths predict opposing reactivity trends.

Metal−Oxygen Bond Strengths versus Metal−Hydrogen Bond Strengths. In the absence of any opposing feature, it may be obvious that the metal−oxygen bond strengths have a profound influence on the different photocatalytic properties of oxygen vacancies on different metal oxide surfaces. For instance, taking the metal−oxygen bond strengths alone into account, we easily ascertain that the different tungsten−oxygen and molybdenum−oxygen bond strengths result in different products obtained. Oxidation was preferred in the case of $W_3O_5^-$ containing the stronger[107] metal−oxygen bonds to form the significantly more stable $W_3O_6^-$ (and liberate hydrogen), whereas $Mo_3O_5^-$ with the weaker metal−oxygen bonds preferred to form a kinetic trap.

Yet, when the metal−hydrogen bond strengths are also taken in consideration,[110] the HHIs containing the more reactive Mo−H bond are in fact expected to more readily lead to hydrogen liberation, completely contradicting the experimental observations. However, the "accessibility factor" (see above) renders the metal−oxygen bond strengths to be more important. In general, therefore, it is expected that oxidation upon reaction with water (accompanied by the liberation of H_2) is energetically more profitable for the TMO with the stronger metal−oxygen bond whenever the metal−hydrogen bond strengths become secondary due to kinetic accessibility issues.

Initially Formed Electrostatic Complexes. In a TMO with several different reactive sites, an incoming small molecule can adopt different orientations with respect to the metal oxide to form several different complexes. To gain a holistic view of subsequent chemical reactivity, and to trace the various reaction pathways which emanate from the different electrostatic complexes it is essential to obtain all these complexes within a favorable energetic window under the experimental conditions. It is also important to carefully study the interconversion between the different complexes. For instance, in this particular study, the kinetic trap formation with $Mo_3O_5^-$ was possible only with the higher-energy complex **C8** which in spite of inherently not being the most populated complex was readily accessed from complex **C2**.

Geometric Factors and Facial Selectivity. Certain geometric factors introduced in the course of a chemical reaction of a TMO with a small molecule preclude the formation of certain isomers and result in unexpected outcomes. For example, in Figure SI_4, all the processes occur only on the top face, and hence a different isomer is formed. Specifically, in our case, it was not of importance as we were able to find a lower-energy pathway. Yet, more generally, it is vital that one is aware of the facial selectivity arising due to certain geometric factors when using TMOs for important processes such as photocatalytic liberation of H_2 from water.

Use of Cluster Models That Closely Mimic the Surface. Liberation of H_2 in the reaction of a metal oxide surface with water usually involves (a) an energetic barrier, (b) some important geometric factors at play, or (c) disparate reactivity patterns with different metals.[111] Cluster models that attempt to model the surfaces need to be consistent with these aspects. Moreover, an additional catalyst or a sacrificial agent is normally required for photocatalytic water splitting, as demonstrated by Sato and White in one of the earliest works on TiO_2 photochemistry.[113] Thus a complete understanding of photocatalytic hydrogen generation warrants the investigation of the role of a cocatalyst. However, in order to even rationally design a suitable catalyst/cocatalyst system in the first place, a

thorough mechanistic knowledge of the individual steps is essential. Appropriate cluster models are very helpful in this regard.

Insights from the Processes That Do Not Occur. In addition to fittingly accounting for the experimental observations, our study illustrates that a complete understanding of the metal dependence in the phenomenon of H_2 liberation emerges only after we satisfactorily explain the non-occurrence of alternate processes as well (vide supra).

Fluxionality Pathway Is a Suitable Beginning Point. When a small molecule (such as water) reacts with a TMO, several reactivity possibilities exist, and in the absence of an appropriate starting pathway, systematically tracing the reaction pathways becomes an onerous task. This is particularly true for larger clusters where there are more possibilities for chemical reactions to happen. However, this study has established that kinetic trap formation and H_2 liberation processes are offshoots of the fluxionality pathway (vide supra). The fluxionality pathway[56,57] is thus a reliable starting point to study the reactivity of small molecules with TMOs.

Careful Assessment of Thermodynamic and Kinetic Factors. It is important to note that kinetic and thermodynamic factors play key roles in determining the differences between Mo oxides and W oxides. As is commonly the case in chemistry, while the qualitative aspects of the reaction mechanisms are similar, it is imperative to assess the quantitative aspects in such situations to confirm which product is obtained in case of a competition. Two specific cases in this work—the thermodynamic stability of **DH4** over **DH3** and how kinetic inaccessibility relegates the metal–hydrogen bond strengths to only be a secondary factor—emphasize the role played by thermodynamic and kinetic aspects, respectively.

Free Energies versus Enthalpies or Energies. It is common practice in the literature to report the reaction pathway in terms of the enthalpies or energies. However, in the reactivity of water with the TMOs, a significant entropic penalty is involved when two molecules (water and the TMO cluster) react to become one molecule. This entropic penalty also suggests that other reaction possibilities such as a cooperative process with the adsorption of an additional water molecule on to the TMO cluster are unlikely.

We find that the entropic penalty is on the order of 8 kcal/mol (see Supporting Information). Also, merely using enthalpies consistently predicts no barriers for most of the reaction pathways in this work, and thus it is very easy to come to the wrong conclusion that a lot of these pathways are feasible. Therefore, we recommend the use of free energies over enthalpies of energies in the reactivities of TMO clusters with water wherein entropy effects are important.

CONCLUSIONS

In this work, the different products obtained in the chemical reactions of $W_3O_5^-$ and $Mo_3O_5^-$ with water help us provide new insights on the key factors involved in the catalytic liberation of H_2 from water using cluster models of transition-metal oxides. The molybdenum oxide cluster in its reaction with water forms a kinetic trap, whereas the tungsten oxide gets oxidized to generate H_2. The kinetic trap obtained from $Mo_3O_5^-$ corresponds to a unique dihydroxide structure. The oxidized product obtained from $W_3O_5^-$ has the same geometry as the lowest-energy isomer of $W_3O_6^-$. Answers to the intriguing questions of what happens and what does not happen in this context teach us significant lessons on the vital roles played by the different metal oxide and metal–hydrogen bond strengths, the electrostatic complexes formed initially, the loss of entropy, and crucial geometric factors involved in the generation of H_2. Overall, the understanding we gain from this study is beneficial for the design of better photocatalysts.

ASSOCIATED CONTENT

Supporting Information

Several reaction energy pathways, the additional functions added to the double-ζ and the triple-ζ basis sets, the Cartesian coordinates of all the optimized structures, and spectroscopic parameters used to generate the simulations shown in Figure 8 are provided in the Supporting Information. This material is available free of charge via the Internet at http://pubs.acs.org.

AUTHOR INFORMATION

Corresponding Author

kraghava@indiana.edu

Notes

The authors declare no competing financial interest.

ACKNOWLEDGMENTS

This work was supported in its entirety by Department of Energy Grant No. DE-FG02-07ER15889. ROR is grateful to Karthik Alagesan for providing the high-resolution image he photographed for a potential cover art and to Benjamin Gamoke for his helpful contributions with the image

REFERENCES

(1) Lewis, N. S.; Nocera, D. G. *Proc. Natl. Acad. Sci. U.S.A.* **2006**, *103*, 15729–15735.
(2) Cook, T. R.; Dogutan, D. K.; Reece, S. Y.; Surendranath, Y.; Teets, T. S.; Nocera, D. G. *Chem. Rev.* **2010**, *110*, 6474–6502.
(3) Sundstrom, E. J.; Yang, X.; Thoi, V. S.; Karunadasa, H. I.; Chang, C. J.; Long, J. R.; Head-Gordon, M. *J. Am. Chem. Soc.* **2012**, *134*, 5233–5242.
(4) Maeda, K.; Domen, K. *J. Phys. Chem. Lett.* **2010**, *1*, 2655–2661.
(5) Lee, J. S. *Catal. Surv. Asia* **2005**, *9*, 217–227.
(6) Maeda, K.; Domen, K. *J. Phys. Chem. C* **2007**, *111*, 7851–7861.
(7) Osterloh, F. E. *Chem. Matter.* **2008**, *20*, 35–54.
(8) Kudo, A.; Miseki, Y. *Chem. Soc. Rev.* **2009**, *38*, 253–278.
(9) Youngblood, W. J.; Lee, S.-H. A.; Maeda, K.; Mallouk, T. E. *Acc. Chem. Res.* **2009**, *42*, 1966–1973.
(10) Maeda, K.; Teramura, K.; Lu, D.; Takata, T.; Saito, N.; Inoue, Y.; Domen, K. *Nature* **2006**, *440*, 295.
(11) Hata, H.; Kobayashi, Y.; Bojan, V.; Youngblood, W. J.; Mallouk, T. E. *Nano Lett.* **2008**, *8*, 794–799.
(12) Maeda, K.; Teramura, K.; Lu, D.; Saito, N.; Inoue, Y.; Domen, K. *Angew. Chem., Int. Ed.* **2006**, *45*, 7806–7809.
(13) Maeda, K.; Teramura, K.; Lu, D.; Saito, N.; Inoue, Y.; Domen, K. *J. Phys. Chem. C* **2007**, *111*, 7554–7560.
(14) Maeda, K.; Sakamoto, N.; Ikeda, T.; Ohtsuka, H.; Xiong, A.; Lu, D.; Kanehara, M.; Teranishi, T.; Domen, K. *Chem.—Eur. J.* **2010**, *16*, 7750–7759.
(15) Sakamoto, N.; Ohtsuka, H.; Ikeda, T.; Maeda, K.; Lu, D.; Kanehara, M.; Teramura, K.; Teranishi, T.; Domen, K. *Nanoscale* **2009**, *1*, 106–109.
(16) Yoshida, M.; Takanabe, K.; Maeda, K.; Ishikawa, A.; Kubota, J.; Sakata, Y.; Ikezawa, Y.; Domen, K. *J. Phys. Chem. C* **2009**, *113*, 10151–10157.
(17) Hisatomi, T.; Maeda, K.; Takanabe, K.; Kubota, J.; Domen, K. *J. Phys. Chem. C* **2009**, *113*, 21458–214666.
(18) For a comprehensive review on solar water splitting cells and the role of transition-metal oxides in it, see: Walter, M. G.; Warren, E. L.; Mckone, J. R.; Boettcher, S. W.; Mi, Q.; Santori, E. A.; Lewis, N. S. *Chem. Rev.* **2010**, *110*, 6466–6473.

(19) Jena, P.; Castleman, A. W., Jr. *Proc. Natl. Acad. Sci. U.S.A.* **2006**, *103*, 10560−10569.
(20) Witko, M.; Hermann, K.; Tokarz, R. *J. Electron Spectrosc. Relat. Phenom.* **1994**, *69*, 89−98.
(21) Muetterties, E. L. *Science* **1997**, *196*, 839−848.
(22) Lai, X.; Goodman, D. W. *J. Mol. Catal. A* **2000**, *162*, 1647−1650.
(23) Gong, Y.; Zhou, M.; Andrews, L. *Chem. Rev.* **2009**, *109*, 6765−6808 and references therein.
(24) Wyrwas, R. B.; Yoder, B. L.; Maze, J. T.; Jarrold, C. C. *J. Phys. Chem. A* **2006**, *110*, 2157−2164 and references therein.
(25) Rothgeb, D. W.; Kuo, A. T.; Troyer, J. L.; Jarrold, C. C.; Mayhall, N. J.; Raghavachari, K. *J. Chem. Phys.* **2009**, *130*, 124314-1-8.
(26) Wyrwas, R. B.; Robertson, E. M.; Jarrold, C. C. *J. Chem. Phys.* **2007**, *126*, 214309-1-8.
(27) Wyrwas, R. B.; Jarrold, C. C. *J. Am. Chem. Soc.* **2006**, *128*, 13688−13689.
(28) Johnson, G. E.; Reveles, J. U.; Khanna, S. N.; Castleman, A. W., Jr. *J. Phys. Chem. C* **2010**, *114*, 5438−5446.
(29) Johnson, G. E.; Mitric, R.; Nossler, M.; Tyo, E. C.; Koutecky, V. B.; Castleman, A. W., Jr. *J. Am. Chem. Soc.* **2009**, *131*, 5460−5470 and references therein.
(30) Johnson, G. E.; Reveles, J. U.; Reilly, N. M.; Tyo, E. C.; Khanna, S. N.; Castleman, A. W., Jr. *J. Phys. Chem. A* **2008**, *112*, 11330−11340.
(31) Johnson, G. E.; Reveles, J. U.; Reilly, N. M.; Castleman, A. W., Jr. *Int. J. Mass Spectrom.* **2009**, *280*, 93−100.
(32) Johnson, G. E.; Tyo, E. C.; Castleman, A. W., Jr. *J. Phys. Chem. C* **2008**, *112*, 9730−9736.
(33) Reilly, N. M.; Reveles, J. U.; Johnson, G. E.; del Campo, J. M.; Khanna, S. N.; Koster, A. M.; Castleman, A. W., Jr. *J. Phys. Chem. C* **2007**, *111*, 19086−19097.
(34) Reilly, N. M.; Reveles, J. U.; Johnson, G. E.; Khanna, S. N.; Castleman, A. W., Jr. *J. Phys. Chem. A* **2007**, *111*, 4158−4166.
(35) Reilly, N. M.; Reveles, J. U.; Johnson, G. E.; Khanna, S. N.; Castleman, A. W., Jr. *Chem. Phys. Lett.* **2007**, *435*, 295−300.
(36) Reilly, N. M.; Johnson, G. E.; Kimble, M. L.; Castleman, A. W., Jr. *J. Am. Chem. Soc.* **2008**, *130*, 1694−1698 and references therein.
(37) Zhai, H. J.; Averkiev, B. B.; Zubarev, D. Yu.; Wang, L. S.; Boldyrev, A. I. *Angew. Chem., Int. Ed.* **2007**, *46*, 4277−4280.
(38) Bondarchuk, O.; Huang, X.; Kim, J.; Kay, B. D.; Wang, L. S.; White, J. M.; Dohnalek, Z. *Angew. Chem., Int. Ed.* **2006**, *45*, 4786−4789.
(39) Huang, X.; Zhai, H. J.; Waters, L. J.; Wang, L. S. *Angew. Chem., Int. Ed.* **2006**, *45*, 657−660.
(40) Huang, X.; Zhai, H. J.; Kiran, B.; Wang, L. S. *Angew. Chem., Int. Ed.* **2005**, *44*, 7251−7254.
(41) Li, S.; Dixon, D. A. *J. Phys. Chem. A* **2007**, *111*, 11093−11099.
(42) Zhai, H. J.; Kiran, B.; Cui, L. F.; Li, X.; Dixon, D. A.; Wang, L. S. *J. Am. Chem. Soc.* **2004**, *126*, 16134−16141.
(43) Zhai, H. J.; Dobler, J.; Sauer, J.; Wang, L. S. *J. Am. Chem. Soc.* **2007**, *129*, 13270−13276.
(44) Bell, R. C.; Zemski, K. A.; Castleman, A. W., Jr. *J. Phys. Chem. A* **1999**, *103*, 1585−1591.
(45) Sun, Q.; Rao, B. K.; Jena, P.; Stolcic, D.; Kim, Y. D.; Gantefor, G.; Castleman, A. W., Jr. *J. Chem. Phys.* **2004**, *121*, 9417−9422.
(46) Li, S.; Zhai, H. J.; Wang, L. S.; Dixon, D. A. *J. Phys. Chem. A.* **2009**, *113*, 11273−11288.
(47) Bergeron, D. E.; Castleman, A. W., Jr.; Jones, N. O.; Khanna, S. N. *Nano Lett.* **2004**, *2*, 261−265.
(48) Zhai, H. J.; Wang, B.; Huang, X.; Wang, L. S. *J. Phys. Chem. A* **2009**, *113*, 9804−9813.
(49) Gustav, G. L.; Jena, P.; Zhai, H. J.; Wang, L. S. *J. Chem. Phys.* **2001**, *115*, 7935−7944.
(50) Zhai, H. J.; Huang, X.; Waters, T.; Wang, X. B.; O'Hair, R. A. J.; Wedd, A. G.; Wang, L. S. *J. Phys. Chem. A* **2005**, *109*, 10512−10520.
(51) Zhai, H. J.; Wang, L. S. *J. Chem. Phys.* **2006**, *125*, 164315-1-9.
(52) Li, S. G.; Dixon, D. A. *J. Phys. Chem. A* **2006**, *110*, 6231−6244.
(53) Li, S. G.; Dixon, D. A. *J. Phys. Chem. A* **2008**, *112*, 6646−6666.
(54) Li, S.; Dixon, D. A. *J. Phys. Chem. C* **2011**, *115*, 19190−19196.
(55) Li, S.; Guenther, C. L.; Kelley, M. S.; Dixon, D. A. *J. Phys. Chem. C* **2011**, *115*, 8072−8103.
(56) Ramabhadran, R. O.; Mayhall, N. J.; Raghavachari, K. *J. Phys. Chem. Lett.* **2010**, *1*, 3066−3071.
(57) Ramabhadran, R. O.; Becher, E. L, III.; Chowdhury, A.; Raghavachari, K. *J. Phys. Chem. A* **2012**, *116*, 7189−7195.
(58) Zhai, H. J.; Zhang, X. H.; Chen, W. J.; Huang, X.; Wang, L. S. *J. Am. Chem. Soc.* **2011**, *133*, 3085−3094.
(59) Dong, F.; Heinbuch, S.; Xie, Y.; Rocca, J. J.; Bernstein, E. R.; Wang, Z. C.; Deng, K.; He, S. G. *J. Am. Chem. Soc.* **2008**, *130*, 1932−1943.
(60) Jackson, P.; Fisher, K. J.; Willet, G. D. *Int. Mass Spectrom.* **2000**, *197*, 95−103.
(61) Jackson, P.; Fisher, K. J.; Willet, G. D. *Chem. Phys.* **2000**, *262*, 179−187.
(62) Fielicke, A.; Meijer, G.; von Helden, G. *Eur. Phys. J. D* **2003**, *24*, 69−72.
(63) Molek, K. S.; Jaeger, T. D.; Duncan, M. A. *J. Chem. Phys.* **2005**, *123*, 144313.
(64) Dong, F.; Heinbuch, S.; He, S. G.; Xie, Y.; Rocca, J. J.; Bernstein, E. R. *J. Chem. Phys.* **2006**, *125*, 164318.
(65) Fialko, E. F.; Kikhtenko, A. V.; Goncharov, V. B.; Zamaraev, K. I. *J. Phys. Chem. B* **1997**, *101*, 5772−5773.
(66) Rothgeb, D. W.; Mann, J. E.; Jarrold, C. C. *J. Chem. Phys.* **2010**, *133*, 054305.
(67) Rothgeb, D. W.; Mann, J. E.; Waller, S. E.; Jarrold, C. C. *J. Chem. Phys.* **2011**, *135*, 104312.
(68) Green, S. M. E.; Alex, S.; Fleischer, N. L.; Millam, E. L.; Marcy, T. P.; Leopold, D. G. *J. Chem. Phys.* **2001**, *114*, 2653.
(69) Gutsev, G. L.; Weatherford, C. A.; Jena, P.; Johnson, E.; Ramachandran, B. R. *Chem. Phys. Lett.* **2013**, *556*, 211.
(70) Pradhan, K.; Gutsev, G. L.; Weatherford, C. A.; Jena, P. *J. Chem. Phys.* **2011**, *134*, 144305.
(71) Gutsev, G. L.; Weatherford, C. A.; Pradhan, K.; Jena, P. *J. Phys. Chem. A* **2010**, *114*, 9014−9021.
(72) Bertram, N.; Kim, Y. D.; Gantefor, G.; Sun, Q.; Jena, P.; Tamuliene, J.; Seifert, J. *J. Chem. Phys.* **2004**, *396*, 341.
(73) Khanna, S. N.; Jena, P.; Zheng, W. J.; Nilles, J. M.; Bowen, K. H. *Phys. Rev. B* **2004**, *69*, 144418.
(74) Sun, Q.; Rao, B. K.; Jena, P.; Stolcic, D.; Kim, Y. D.; Gantefor, G.; Kawazoe, Y. *Chem. Phys. Lett.* **2004**, *387*, 29−34.
(75) Gutsev, J. L.; Jena, P.; Zhai, H. J.; Wang, L. S. *J. Chem. Phys.* **2001**, *115*, 7935−7944.
(76) Reber, A. C.; Khanna, S. N.; Tyo, E. C.; Harmon, C. L.; Castleman, A. W., Jr. *J. Chem. Phys.* **2011**, *135*, 234303.
(77) Tyo, E. C.; Castleman, A. W.; Reber, A. C., Jr.; Khanna, S. N. *J. Phys. Chem. C* **2011**, *115*, 16797−16802.
(78) Jones, N. O.; Reddy, B. V.; Rasouli, F.; Khanna, S. N. *Phys. Rev. B* **2005**, *72*, 165411.
(79) Wang, T.-H.; Fang, Z.; Gist, N. W.; Li, S.; Dixon, D. A.; Gole, J. L. *J. Phys. Chem. C* **2011**, *115*, 9344−9360.
(80) Fang, Z.; Outlaw, M.; Smith, K.; Gist, N.; Li, S.; Dixon, D. A.; Gole, J. L. *J. Phys. Chem. C* **2012**, *116*, 8475−8492.
(81) Fang, Z.; Dixon, D. A. *J. Phys. Chem. A* **2013**, *117*, 3539−3555.
(82) For some applications of non-transition-metal oxide clusters as models for probing the role of surface defects in catalysis, see refs 82−87. Guevara-Garcia, A.; Martinez, A.; Ortiz, J. V. *J. Chem. Phys.* **2005**, *122*, 214309.
(83) Tenorio, F. J.; Murray, I.; Martinez, A.; Klabunde, K. J.; Ortiz, J. V. *J. Chem. Phys.* **2004**, *120*, 7955−7962.
(84) Martinez, A.; Tenorio, F. J.; Ortiz, J. V. *J. Phys. Chem. A* **2003**, *107*, 2589−2595.
(85) Martinez, A.; Sansores, L. E.; Salcedo, R.; Tenorio, F. J.; Ortiz, J. V. *J. Phys. Chem. A* **2002**, *106*, 10630−10635.
(86) Martinez, A.; Tenorio, F. J.; Ortiz, J. V. *J. Phys. Chem. A* **2001**, *105*, 8787−8793.
(87) Martinez, A.; Tenorio, F. J.; Ortiz, J. V. *J. Phys. Chem. A* **2001**, *105*, 11291−11294.

(88) Mayhall, N. J.; Rothgeb, D. W.; Hossain, E.; Jarrold, C. C.; Raghavachari, K. *J. Chem. Phys.* **2009**, *131*, 144302.
(89) Rothgeb, D. W.; Hossain, E.; Mann, J. E.; Jarrold, C. C. *J. Chem. Phys.* **2010**, *131*, 064302.
(90) Moravec, V. D.; Jarrold, C. C. *J. Chem. Phys.* **1998**, *108*, 1804.
(91) Dietz, T. G.; Duncan, M. A.; Powers, D. E.; Smalley, R. E. *J. Chem. Phys.* **1981**, *74*, 6511.
(92) Davico, G. E.; Schwartz, R. L.; Ramond, T. M.; Lineberger, W. C. *J. Phys. Chem. A* **1999**, *103*, 6167.
(93) Frisch, M. J.; Trucks, G. W.; Schlegel, H. B.; Scuseria, G. E.; Robb, M. A.; Cheeseman, J. R.; Scalmani, G.; Barone, V.; Mennucci, B.; Petersson, G. A.; Nakatsuji, H.; Caricato, M.; Li, X.; Hratchian, H. P.; Izmaylov, A. F.; Bloino, J.; Zheng, G.; Sonnenberg, J. L.; Hada, M.; Ehara, M.; Toyota, K.; Fukuda, R.; Hasegawa, J.; Ishida, M.; Nakajima, T.; Honda, Y.; Kitao, O.; Nakai, H.; Vreven, T.; Montgomery, J. A., Jr.; Peralta, J. E.; Ogliaro, F.; Bearpark, M.; Heyd, J. J.; Brothers, E.; Kudin, K. N.; Staroverov, V. N.; Kobayashi, R.; Normand, J.; Raghavachari, K.; Rendell, A.; Burant, J. C.; Iyengar, S. S.; Tomasi, J.; Cossi, M.; Rega, N.; Millam, J. M.; Klene, M.; Knox, J. E.; Cross, J. B.; Bakken, V.; Adamo, C.; Jaramillo, J.; Gomperts, R.; Stratmann, R. E.; Yazyev, O.; Austin, A. J.; Cammi, R.; Pomelli, C.; Ochterski, J. W.; Martin, R. L.; Morokuma, K.; Zakrzewski, V. G.; Voth, G. A.; Salvador, P.; Dannenberg, J. J.; Dapprich, S.; Daniels, A. D.; Farkas, A. ; Foresman, J. B.; Ortiz, J. V.; Cioslowski, J.; Fox, D. J. *Gaussian 09*, revision A.1; Gaussian Inc.: Wallingford, CT, 2009.
(94) Becke, A. D. *J. Chem. Phys.* **1993**, *98*, 5648−5652.
(95) Lee, C. T.; Yang, W. T.; Parr, R. G. *Phys. Rev. B* **1988**, *37*, 785−789.
(96) Andrae, D.; Hausserman, U.; Dolg, M.; Stoll, H.; Preuss, H. *Theor. Chem. Acc.* **1990**, *77*, 123−141.
(97) Dunning, T. H., Jr.; Hay, P. J. In *Modern Theoretical Chemistry*; Schaefer, H. F., Ed.; Plenum Press: New York, 1976; Vol. 3, pp 1−28.
(98) Kendall, R. A.; Dunning, T. H., Jr.; Harrison, R. J. *J. Chem. Phys.* **1992**, *96*, 6796−6806.
(99) Zhao, Y.; Truhlar, D. G. *Theor. Chem. Acc.* **2008**, *120*, 215−241.
(100) Since the spectra shown were collected at room temperature, some signal due to hot band transitions appears at binding energies below what we believe is the ADE. Hot band signal can be discerned from "cold" signal because of its variation with source temperature, and sequence bands can contribute to apparent peak intensities in ways that are modeled well by spectral simulations. By comparing relative intensities of signal near the band origin under different source conditions, we have ascertained that signal below 1.984 eV is due to hot band transitions. Thus, overall, the intensity of signal found to binding energy below 1.984 eV was found to be sensitive to source conditions (such as ion temperature). This observation, combined with simulations, therefore narrowed the assignment of the ADE to 1.984 eV.
(101) Grimme, S.; Antony, J.; Ehlrich, S.; Krieg, H. A *J. Chem. Phys.* **2010**, *132*, 154104.
(102) More precisely, we get the mirror image of DH3 when we start with complex C6 (Figure SI_3). Since we do not deal with any chiral aspect here, for the sake of clarity, we do not make a distinction between these mirror images and call both DH3 and its mirror image as DH3 only.
(103) Ervin, K. M. PESCAL, Fortran program (2010). The interested reader can access the program from the following website: http://wolfweb.unr.edu/~ervin/pes/.
(104) Ervin, K. M.; Ramond, T. M.; Davico, G. E.; Schwartz, R. L.; Casey, S. M.; Lineberger, W. C. *J. Phys. Chem. A* **2001**, *101*, 10822−108831.
(105) Rothgeb, D. W.; Hossain, E.; Kuo, A. T.; Troyer, J. L.; Jarrold, C. C. *J. Chem. Phys.* **2009**, *131*, 044310.
(106) For one of the earliest papers explaining kinetic shift, see: Friedman, L.; Long, F. A.; Wolfsberg, M. *J. Chem. Phys.* **1957**, *26*, 714.
(107) Li, S. G.; Hennigan, J. M.; Peterson, K. A.; Dixon, D. A. *J. Phys. Chem. A* **2009**, *113*, 7861−7877.
(108) Chai, J.-D.; Head-Gordon, M. *Phys. Chem. Chem. Phys.* **2008**, *10*, 6615−6620.
(109) Tao, J. M.; Perdew, J. P.; Starvoverov, V. N.; Scuseria, G. E. *Phys. Rev. Lett.* **2003**, *91*, 146401−146404.
(110) Uddin, J.; Morales, C. M.; Maynard, J. H.; Landis, C. *Organometallics* **2006**, *25*, 5566−5581.
(111) Somorjai, G. A.; Li, Y. *Introduction to Surface Chemistry and Catalysis*; John Wiley & Sons: Hoboken, NJ, 2010.
(112) Standard Thermodynamic Properties of Chemical Substances. In *CRC Handbook of Chemistry and Physics*, 93rd ed. (Internet version); Haynes, W. M., Ed.; CRC Press/Taylor and Francis: Boca Raton, FL, 2013.
(113) Sato, S.; White, J. M. *J. Am. Chem. Soc.* **1980**, *102*, 7206−7210.